Advanced Composites and Hybrid Materials (2025) 8:167
https://doi.org/10.1007/s42114-025-01255-8

RESEARCH

Highly porous hollow 3D devices obtained by a combined melt-wet processing for long-term controlled release

Marta Balsamo[1,2] · Maria Chiara Mistretta[1,2] · Roberto Scaffaro[1,2]

Received: 18 June 2024 / Revised: 8 January 2025 / Accepted: 28 January 2025

Abstract

The possibility to obtain resistant and reusable hollow devices with differentiated high porosity for storage and tunable long-term controlled release of substances is difficult to achieve efficiently. To solve this problem, we propose a combined melt-wet processing, which allows predictable and tunable morphologies. The process consists in combining Material Extrusion (MEX) with an eco-friendly salt leaching in distilled water, by using a biostable polymer and high percentages of saline porogen. Three blends with PA6/NaCl-30/70wt% composition were extruded, varying the salt particles size, that shows good dispersion in all the filaments, with a spontaneous tendency for bigger particles to accumulate in the central region of the cross-sections, attributable to fluid-dynamic reasons. Blends rheological and mechanical properties appeared suitable for the printing process. The hollow devices were then printed and successfully leached, resulting in homogeneously dispersed pores, with size ranges comparable to those of the porogen for each blend; therefore, the morphology of the pores can be directly predicted by the porogen and it was not altered during processing. Leaching occurred completely, in fact the real porosity for each device was consistent with the theoretical one. Despite the high percentage of voids, the hollow devices appeared to be mechanically resistant and therefore suitable for the application. Controlled release up to 11 days of a model molecule (methylene blue) was tested and predictable kinetics related to pore size were achieved so, therefore, they are easily tunable and versatile. Release data were fitted according to Peppas-Korsmeyer-model to describe the release mechanism related to porosity.

Keywords 3D printing · Selective leaching · Porosity · Controlled release · Reservoir-type

Highlights
- Combined process of MEX and salt leaching to achieve high porosity and versatility.
- PA6/NaCl 30/70%wt blends, with biostable polymer and different salt granulometry.
- Predictability of pore morphology and possibility of achieving porosity gradients.
- Production of reusable porous devices for tunable long-term controlled release.
- Possibility of adjusting release kinetics through easy changes in porogen size.

✉ Maria Chiara Mistretta
mariachiara.mistretta@unipa.it

✉ Roberto Scaffaro
roberto.scaffaro@unipa.it

Marta Balsamo
marta.balsamo01@unipa.it

[1] Department of Engineering, University of Palermo, Viale Delle Scienze, 90128 Palermo, Italy

[2] Consortium for Materials Science and Technology, INSTM, Via Giusti 9, 50125 Florence, Italy

1 Introduction

Optimization in the production of porous systems represents a multidisciplinary innovation frontier, as these currently occupy leading roles in different applications, as biodegradable or biostable systems [1–4]. Porous systems, in fact, can be used for the controlled release of substances as the percentage of porosity and the type of porosity allow significant influence on the kinetics of their release, enabling regulation and adaptation to specific needs. Controlled release typically involves drugs and results in the ability to regulate the concentration of the drug in some parts of the body over others [5]. Besides drugs, porous devices have recently been used to release also hormones or other biomolecules to treat chronic diseases, such as diabetes [6]. In addition to controlled release of drugs or hormones, which is useful in advanced pharmaceutical therapies, controlled release of fertilizers and pesticides is gaining importance nowadays, as it plays a substantial role in sustainable agriculture [7–9].

Published online: 11 February 2025

Among the possible modes of controlled release of substances by porous devices, a possible distinction can be made between monolithic-type devices, in which the substance is homogeneously dispersed in the matrix, and reservoir-type devices, in which the material acts as a capsule containing the substance [10]. The latter case has advantages over the former, in terms of the possibility of refilling and reusing the device, if biostable. In addition, the substance can be loaded after the production of devices, so it will not be subjected to the material processing, which could alter its functionality. These are hollow structures, generally cylindrical or discoidal in shape, biodegradable or biostable, depending on the duration of the application [11, 12]. The main problem with this type of structure is that the device will have to be handled during filling, so it will have to be mechanically resistant and, at the same time, it will need sufficient porosity to ensure the release of the substance with predictable kinetics. The production of hollow body with differentiated porosity suitable for encapsulation and controlled release is a major processing problem to date. Simplifying their production and improving their performance is, therefore, a particularly relevant area of research.

Among the methods of processing polymeric materials, Material Extrusion (MEX) additive manufacturing process offers advantages related to simplicity and cost-effectiveness [13], and also enables the production of porous devices by adjusting CAD and printing parameters. However, this technology is limited by resolution limits, which restrict the range of pores and porosities achievable to those guaranteed by the printer's performance [14, 15]. Combining this process with equally simple methods, such as selective leaching of porogens, would make it possible to create additional porosity regulated by the porogen. Furthermore, the use of saline porogens such as sodium chloride (NaCl) could be extremely advantageous and green, as it is easily available and processable, and soluble in simple distilled water: in fact, it is widely used in combination with other processes [16–19].

The use of salt leaching in conjunction with MEX, definable as a combined melt-wet processing, therefore, is an innovative and advantageous field, but not so much explored, probably due to difficulties in identifying the most correct process parameters for polymer/salt blends at elevate salt percentage. For this reason, there are few works on this subject in current data and, in any case, the porosity values remain low: Devarshi Kashyap et al. [20], produced a porous system for endovascular applications with a porosity of 32–36%; González-Henríquez et al. [21], worked on the production of a polycaprolactone polycaprolactone-based scaffold achieving an overall porosity of 42%; Teerasuchai et al. [22], achieved porous polybutylene succinate structures for drug delivery, with a maximum of 40/60 wt% polymer/salt; Kosorn Wasana et al. [23], produced cartilage scaffolds based on polycaprolactone, using NaCl as porogen, at 50/50 wt% polymer/salt. In other works, however, non-melt MEX techniques are used with salt leaching, which allow for high porosity percentages but generally require multiple steps and solvent to prepare the ink, [24, 25].

Based on our current understanding to date, there are no studies on the use of this combined technology for the production of hollow device with differentiated porosity, which could be extremely advantageous for all the reasons seen above. In this regard, we propose the production of biostable polyamide 6-based porous hollow device for the storage and long-term controlled release of substances, combining MEX and NaCl leaching. In order to achieve high porosity percentages, we used PA6/NaCl blends at 30/70 wt%, which, to the best of our knowledge, have not been processed in any work to date. In addition, we made three different mixtures, varying the granulometry of the salt, in order to demonstrate the predictability of the pore size and of the release kinetics. The mixtures were extruded and the filaments were printed in devices that appear porous after leaching. Morphological, chemical and mechanical characterizations were conducted before and after printing and before and after leaching in order to analyze the properties of the blends and devices. Finally the release kinetics of methylene blue, selected as a model molecule, was evaluated, to demonstrate the possibility of using them as reusable and tunable controlled release reservoir-type devices.

2 Materials and methods

2.1 Materials

The raw materials used in this work were polyamide 6 (PA6) (Radilon S35 100 NAT, $\rho_{Ny6} = 1.14$ g/cm3), as matrix, and sodium chloride (NaCl) (Fluka, Honeywell, $\rho_{NaCl} = 2.16$ g/cm3), as porogen.

NaCl was processed in three different ways in order to produce three samples with different particles dimensions. The prepared three samples were coded on the base of NaCl size fraction: NaCl_A, produced by Bimby TM6 (Vorwek, Germany), with particles diameter ranging between 1 and 250 µm; NaCl_B supplied by halotherapy centre 'Gemme di Sale—Benessere naturale' in Palermo, with particles diameter ranging between 0.5 and 50 µm; NaCl_C produced by Universal Mill M 20 (IKA, Germany) with particles diameter ranging between 0.5 and 15 µm. Detailed size distributions of NaCl particles are reported in Fig. S1.

All materials were vacuum dried for 24 h at 120 °C in order to avoid hydrolytic degradation of the polymeric matrix during processing.

Table 1 Filaments prepared by extrusion of PA6/NaCl in different porogen granulometry

Sample Code	Matrix	Porogen	Granulometry of Porogen [μm]
Fil_A	PA6 30%	NaCl_A 70%	1.0—275
Fil_B	PA6 30%	NaCl_B 70%	0.5—50
Fil_C	PA6 30%	NaCl_C 70%	0.5—15

2.2 Filaments processing

Both PA6 and PA6/NaCl filaments in the three blends were produced by extrusion using HAAKE Minilab II (Thermo Scientific, USA). Initially, the extrusion of PA6 was conducted in order to establish the most suitable process parameters. PA6 was extruded in flushing mode at a temperature of 240 °C, a pressure of 6 bar and screws speed of 50 rpm. PA6/NaCl, with composition 30/70%wt, were mixed and extruded in recirculating mode, for each NaCl sample. Specifically, 8 g of material (2.4 g of PA6 and 5.6 g of NaCl) was extruded at a temperature of 260 °C, a pressure of 6 bar, screws speed of 50 rpm and recirculating time of 1 min, producing three different filaments, namely Fil_A, Fil_B and Fil_C. PA6/NaCl filaments compositions are summarized in Table 1.

The salt percentage was selected as 70% because, in our previous works, blends with similar polymer/porogen composition ensured adequate porogen leaching and high porosity, although processed differently [16, 26]. All filaments produced have diameters of 1.75 mm, suitable for the 3D printer. Finally, PA6/NaCl filaments produced were subjected to a selective leaching process in 100 ml of distilled water, on a magnetic plate at 80 °C for 24 h at 750 rpm, to remove the porogen NaCl. This process is followed by a final vacuum drying at 120 °C for 24 h.

2.3 Fabrication of 3D printed devices

The porous hollow devices (HD), coded HD_A, HD_B and HD_C, were produced by Material Extrusion (MEX) additive manufacturing process (Sharebot Next Generation, Nibionno) of previously extruded blends filaments Fil_A, Fil_B and Fil_C respectively, after a preliminary analysis conducted on PA6 filaments. Fusion 360 CAD software (Autodesk, USA) was used for 3D modeling and the open source Slic3r software was used for model slicing. The aim was to produce cylindrical hollow devices with inner diameter of 7 mm, height of 5 mm, base thickness of 1 mm and lateral wall thickness of 1 mm, dimensions chosen in relation to similar systems in scientific literature [11]. The optimal process parameters chosen for all blends were: T nozzle 250 °C, T plate 80 °C, extrusion flow rate from the nozzle 37.5 – 35 – 32.5 mm3/s, printing speed 10 mm/s and glue stick (Pritt, Germany) on rough plate. A summary is provided in Table 2.

Finally, the devices produced were subjected to the same selective leaching and vacuum drying process of the filaments. Figure 1 shows the CAD model of the device (a), and its printed, leached and dried version from the front (b) and from the top (c).

2.4 Morphological analysis

The morphology of salt particles, filaments, and devices was evaluated by scanning electron microscopy SEM Phenom ProX (Thermo Scientific, USA). As regards filaments, the morphology of the lateral surface and section, before and

Table 2 Process parameters for PA6/NaCl filaments printing

Sample Code	T nozzle [°C]	T plate [°C]	Flow rate mm3/s	Speed mm/s	Glue	Rough Plate
HD_A	250	80	37.5	10	+	+
HD_B	250	80	35	10	+	+
HD_C	250	80	32.5	10	+	+

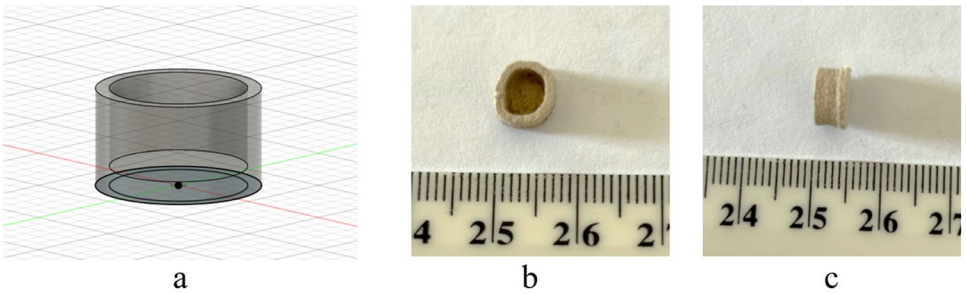

Fig. 1 CAD model the cylindrical hollow devices **a**; leached and dried PA6/NaCl device from the front **b** and from the top **c**

after leaching, was assessed. The sections were obtained by manual fracture under liquid nitrogen. Subsequently, the morphology of printed and leached devices was evaluated, on lateral surface and section; the latter was obtained by cutting with a scalpel between the layers deposited by MEX. The open-source image processing software ImageJ, was used to evaluate the diameter size distribution of particles and pores. For each system, 100 diameters on three different images were considered.

2.5 Rheological characterization

The rheological tests were conducted using a rotational rheometer (ARES-G2, TA Instruments, USA), in frequency sweep mode, in order to assess the processability of blends. All the tests were performed at 240 ◦C in the range 1–100 rad/s. The circular specimens tested were obtained by compression molding with Carver press, at 240 °C, 275 bar and 1 min holding. All blends were tested and complex viscosity as a function of angular frequency has been reported.

2.6 Mechanical properties

The mechanical behavior was assessed by tensile test for the unleached extruded filaments, in order to assess the printability of blends, and by compression in air and wet at 37 °C (BioPuls Bath (Norwood, MA)) for the leached printed devices, in order to simulate the operational conditions of hollow devices, by using an Instron 3365 machine (UK).

Tensile tests were performed on seven filaments of 9 cm for each blend, using a double crosshead speed: 1 mm/min until 2 mm and 100 mm/min until fracture occurred. Elastic modulus, breaking stress and elongation at break have been reported as average values ± standard deviations.

Compressive tests were performed on seven leached devices for each blend in dry and sevens leached devices in wet, using a uniform strain rate of 1 mm min-1. Compressive tests were conducted along the direction in which the device is sealed, thus the most mechanically stressed direction, which is the direction normal to the base. In order to prepare samples to measurements in wet, scaffolds were left in distilled water at 37 °C for 5 min to stabilize the system. Stiffness has been reported as average value ± standard deviation.

2.7 Differential scanning calorimetry (DSC)

The thermal behavior of PA6 and of PA6/NaCl leached blends subjected to the various extrusion/leaching processes was investigated by differential scanning calorimetry (DSC), in order to assess any changes in crystallinity to be attributed to processing. Specimens were analyzed in Chip-DSC 10 (Linseis Thermal Analysis, Germany), according to the following thermal program: first heating from T ambient to 260◦C (3 min hold), cooling to 30◦C (3 min hold), and second heating to 260◦C, all steps at 10◦C/min. The degree of crystallinity (X_c) of the samples was calculated according to equation [27]:

$$X_c = \frac{\Delta H_m}{\Delta H_m^0} \times 100 \quad (1)$$

where ΔH_m represents the experimental enthalpy of melting of the sample (J/g), ΔH_m^0 is the enthalpy of melting for 100% crystalline PA6 (J/g), taken as 230 J/g [28].

2.8 Porosimetry

Porosity of devices has been obtained by various methods, in order to evaluate the effectiveness of leaching, by comparing theoretical and real porosities. First, theoretical porosity P_{Th} was calculated according to equation [29]:

$$P_{Th}\% = \frac{\frac{m_{NaCl}}{\rho_{NaCl}}}{\frac{m_{NaCl}}{\rho_{NaCl}} + \frac{m_{PA6}}{\rho_{Ny6}}} \times 100 \quad (2)$$

where m_{NaCl} and m_{PA6} are NaCl mass and PA6 mass respectively, considering total blend mass of 100 g and PA6:NaCl ratio equal to 70:30; ρ_{NaCl} and ρ_{PA6} are NaCl density and Pa6 density respectively, values known by materials' providers (ρ_{PA6} = 1.14 g/cm3 and ρ_{NaCl} = 2.16 g/cm3). This value represents the case of complete leaching.

Subsequently, the real porosity P_{Grav} of each device was obtained by gravimetric analysis, according to equation:

$$P_{Grav}\% = \frac{\frac{m_{0NaCl}}{\rho_{NaCl}}}{\frac{m_{0NaCl}}{\rho_{NaCl}} + \frac{m_{0PA6}}{\rho_{PA6}}} \times 100 \quad (3)$$

where m_{0PA6} is the mass of the devices after leaching and drying obtained from a precision balance and is the mass of salt lost during leaching, namely, the difference between the mass of the devices before and after leaching and drying.

Porosimetry investigation was also conducted using Pycnometry (Thermo Pycnomatic Helium Pycnometer (Pycnomatic ATC, Thermo Fisher, USA), by obtaining effective density $\rho_{E.Pa6}$, i.e. the calculated and real density of devices. Real porosity P_{Pycno} was obtained according to equation:

$$P_{Pycno}\% = \frac{\frac{m_{NaCl}}{\rho_{NaCl}}}{\frac{m_{NaCl}}{\rho_{NaCl}} + \frac{m_{Pa6}}{\rho_{E.Pa6}}} \times 100 \quad (4)$$

where the terms in the equation have the meanings seen above.

2.9 In vitro controlled release and kinetic models

Substance release performance from device pores was evaluated by in vitro controlled release test of a model molecule, easy to track; leached and dried devices were entirely filled in their internal volumes with a solution based on methylene blue (MB) purchased by Sigma-Aldrich and distilled water, at a concentration of 500 mg/L (≈ 0.15 ml). Following the filling of solution, the devices were sealed with melted PA6 pellets. Model drug release was tested using a UV–Vis spectrophotometer (model UVPC 2401, Shimadzu Italia s.r.l., Milan, Italy). The release of MB was investigated by immersing each device in 10 mL of distilled water at 25◦C. The absorbance band intensity of the solutions was measured at specific time points (1, 2, 3, 4, 24, 48, 72, 96, 168, 264 h) by spectrophotometry at 660 nm [30].

The mechanism of release from the different devices was analyzed by fitting zero order, first order, Higuchi and Korsmeyer-Peppas models to the experimental data in the range of burst region ($M_t/M_\infty < 60\%$) [30–32].

The zero-order kinetics model assumes that drug release is constant, according to equation:

$$M_t = M_0 + k_0 t \tag{5}$$

where M_t and M_0 are the cumulative amounts of drug release at time t and initial time, respectively, and k_0 is the zero order constant.

First-order kinetics model follows equation:

$$M_t = M_\infty (1 - e^{-k_1 t}) \tag{6}$$

where M_∞ is the value of cumulative mass released at plateau and k_1 is the first-order release constant.

The Higuchi model uses equation:

$$M_t = M_0 + k_H t^{0.5} \tag{7}$$

where k_H corresponds to the Higuchi constant.

Finally, the obtained release data were fitted according to Peppas-Korsmeyer equation:

$$\frac{M_t}{M_\infty} = k_p t^n \tag{8}$$

where k_P is the molecule transport constants and n is the transport exponents.

For each model, the respective kinetics constants were evaluated and the statistical parameter R^2 was used to select the most suitable model.

3 Results and discussion

As first inspection to filaments, the morphology of the extruded cross-sections and lateral surfaces of PA6/NaCl blends before leaching and the corresponding particles diameter distributions are shown in Fig. 2.

Specifically, Fig. 2a–c shows the cross-sections of the extruded Fil_A, Fil_B and Fil_C, respectively and Fig. 2a'–c' shows the respective lateral surfaces. In all the samples, salt particles appear well distributed, as sign of good mixing. In addition, voids generated by pull-out of salt particles are present in the sections before leaching, probably due to poor interfacial adhesion between matrix and porogen. It is immediately apparent that particles size is smaller in lateral surfaces area than in the cross-sectional area, for all PA6/NaCl blends: this apparently surprising trend is consistent with the scientific literature [22] and it is attributable to the tendency of particles to migrate laterally towards the centre when subjected to a Poiseuille flow within the extruder; furthermore, there is a correlation between this tendency and particle size, which means that larger particles tend to accumulate in the central area and smaller particles remain close to the wall [33]. This condition is interesting, as it spontaneously generates a porosity gradient along the section.This trend is also confirmed on a quantitative level, in fact particles size distribution histograms are also shown in all cases: for each blend, the particle sizes in the cross-section are always significantly larger than those in the lateral surfaces, as expected; furthermore, for each blend the distribution range of pores in cross-sections remains similar to the salt size range before extrusion, which can be found in Table 1. These results show that processing does not cause fragmentation or agglomeration of particles, so the pores have a predictable size in all the blends.

Figure 3 shows the morphology of the extruded cross-sections and lateral surfaces of PA6/NaCl blends after leaching and the corresponding pores diameter distributions.

Specifically, Fig. 3a–c shows the cross-sections of the extruded Fil_A, Fil_B and Fil_C blends after leaching, respectively and Fig. 3a'–b' shows the respective leached lateral surfaces. Both qualitatively through visual inspections and quantitatively by histograms, it is confirmed that the pores size is larger in the cross-sections than on the lateral surfaces, according to Fig. 2; furthermore, in the histograms, it can be seen that the range of pores distribution is similar to that of the salt prior to leaching, thus, as expected, the pores size is predictable. A summary of pores and porogen statistic based index of the distribution in the systems is reported in Table S1, where the size range in maximum and minimum values, average diameters and

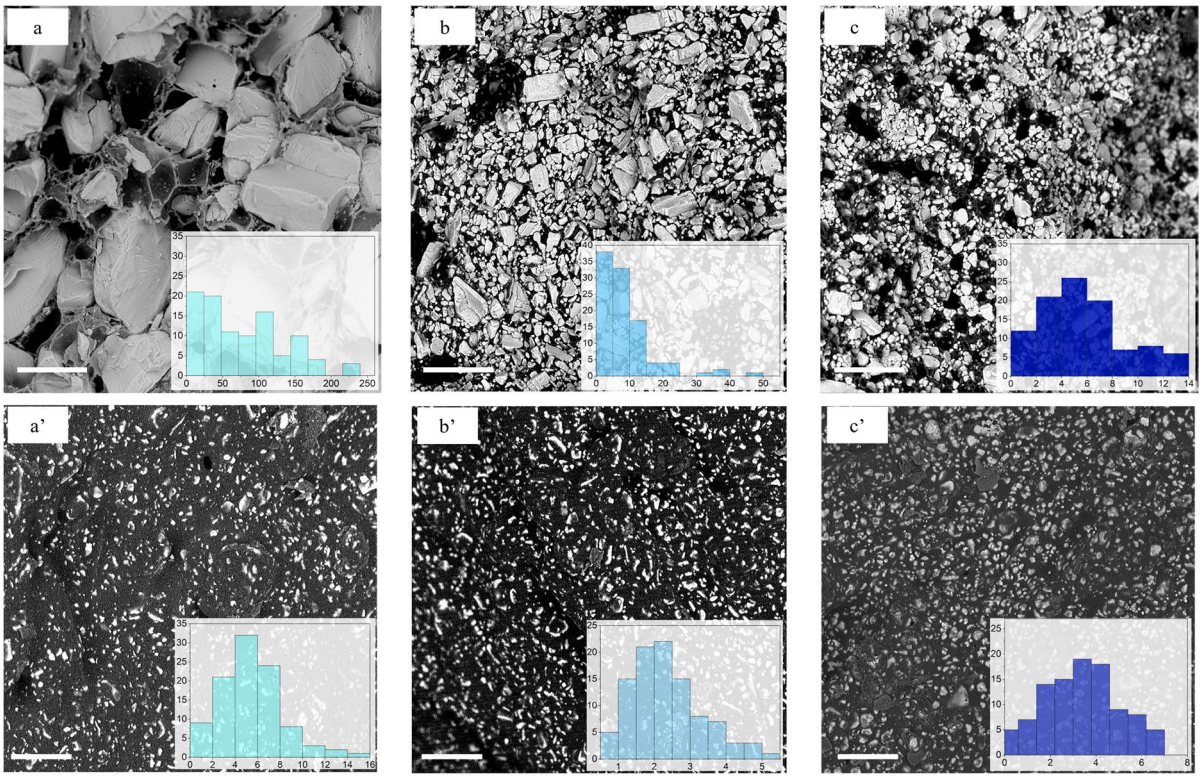

Fig. 2 SEM images of extruded filaments and histograms of particles' diameter distributions: Fil_A (**a**), Fil_B (**b**), Fil_C (**c**) cross-sections and Fil_A (a'), Fil_B (b'), Fil_C (c') lateral surfaces. Scale bar is 100 µm

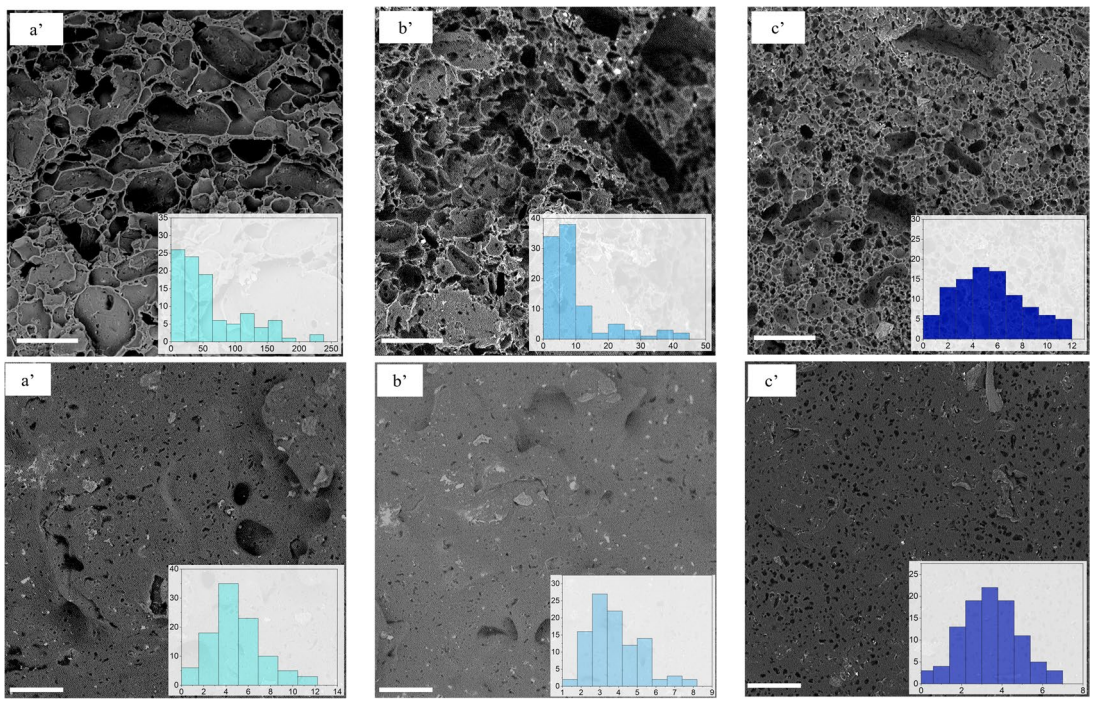

Fig. 3 SEM images of extruded filaments and histograms of pores' diameter distributions: Fil_A (**a**), Fil_B (**b**), Fil_C (**c**) cross-sections after leaching and Fil_A (a'), Fil_B (b'), Fil_C (c') lateral surfaces after leaching. Scale bar is 100 µm

standard deviation values for each system were reported, showing values consisten with those expressed so far. The larger and rounded pores visible in lateral surfaces are probably surface irregularity due to the extrusion process. Finally, no residual porogen can be found in the images, so it is possible to confirm that the leaching was substantially complete.

The adequate distribution of the porogen within the filaments and the possibility of complete leaching revealed by the morphological characterization, confirm that they could be suitable for the production of porous devices. Therefore, following scientific literature [34], rheological tests were carried out by rotational rheometer, to analyze the printing behavior of PA6/NaCl blends and the results are reported in Fig. 4. Since it is known that the Cox-Merz rule is not applicable in systems with high filler content [35], we refer to the complex viscosity trend. It allows an internal comparison between systems and, therefore, enables useful assessments of processability of systems with and without porogen and with different morphology of the latter [35]. It was useful to make a comparison with PA6 to assess how the presence of salt changed the viscosity of the matrix and, consequently, its processability.

PA6 exhibits substantial Newtonian behavior in the investigated frequency range, characterized by an almost constant complex viscosity, as reported in literature [36]. Adding salt induces a non-Newtonian behavior and a general increase in complex viscosity in the whole frequency range for all the samples, showing a predictable relationship of the properties with the presence of porogen in the blends [37]. This is a known behavior, in fact increased complex viscosity is generally attributed to a strong interaction between the dispersed

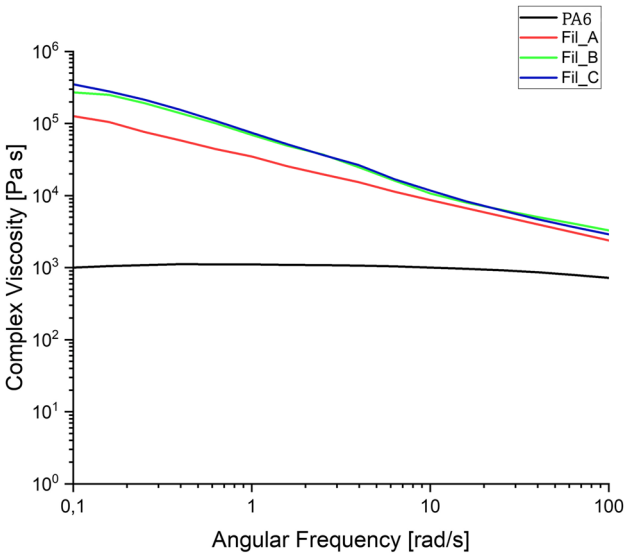

Fig. 4 Complex viscosity as a function of angular frequency for PA6 and PA6/NaCl blends

filler and the matrix that restricts the movement of the polymer chain, as already observed in similar systems [38–40]; similarly, the non-Newtonian behavior is also attributable to matrix-filler interactions and to the larger number of interactions [41, 42]. Complex viscosity tends to increase as particle size decreases, because larger salt particles have a smaller specific surface area, so the interactions degree with the polymer chain is low, resulting in lower complex viscosity [43]. This difference is attenuated at higher frequencies, where the interactions between the polymer matrix and salt have less time to develop and affect viscosity. In particular, the behavior of blends tends to approach the behavior of PA6 alone. This decrease in complex viscosity at high frequencies is advantageous, as it can facilitate the extrusion step from the 3D printer nozzle, where shear rates are typically high [44], making it similar to the printing conditions of PA6. Finally, it is noted that Fil_B and Fil_C exhibit very similar behavior and properties, as expected because of the similar range salt size.

In addition to melt properties, printability was also assessed through mechanical tests on the filaments. Tensile tests were carried out on the extruded PA6 and PA6/NaCl blends to evaluate the differences in mechanical performance due to the presence of the three salt samples in the PA6 matrix and, therefore, the possibility of printing them; the results of elastic modulus, breaking stress and elongation at break are reported in Table 3.

PA6 nature is completely changed by the presence of NaCl. In fact, there is a stiffening of the material, i.e., an increase in its elastic modulus. This can be due to a combination of two synergistic effects: firstly salt particles can act as mechanical reinforcements for the material and, secondly, it could occur an increasing in cristallinity caused by a possible nucleating effect due to the presence of salt particles.The latter phenomenon was explored by DSC tests, conducted in order to assess any changes in crystallinity in the material as a result of the processing and of the presence of the porogen. Results are reported in Table 4.

As expected, there is a slight increase in the degree of crystallinity X_c in the blends that contained the salt, likely due to the nucleating effect of the particles; furthermore, the increase in crystallinity is greater when the salt particles

Table 3 Results from tensile test conducted on PA6 and PA6/NaCl blends filaments, in terms of Elastic Modulus, Breaking Stress and Elongation at Break

	Elastic Modulus [MPa]	*Breaking Stress [MPa]*	*Elongation at Break %*
PA6	1503.2 ± 67.2	69.5 ± 7.9	41.1 ± 2.1
Fil_A	3578.7 ± 204.0	15.9 ± 1.3	0.6 ± 0.1
Fil_B	2794.1 ± 226.7	12.5 ± 1.0	0.6 ± 0.1
Fil_C	2346.4 ± 307.1	11.5 ± 1.5	0.8 ± 0.3

Table 4 Results of DSC tests conducted on PA6 and PA6/NaCl leached blends

	PA6_pellet	PA6	Fil_A leached	Fil_B leached	Fil_C leached
ΔH_m [mJ/mg]	40.0	41.0	49.5	53.9	56.2
X_c [%]	17%	18%	22%	23%	24%

are smaller in size, beacuse smaller particle size provides more crystallization nuclei, which more effectively increased the crystallinity of the composites [45]. Elastic modulus is expected to increases as the particle size decreases, because for the same percentage of filler, smaller particles have more surface area and greater interactions with the matrix, but surprisingly the opposite occurs, in fact, values increase with increasing particles. This could be justified considering the poor interfacial adhesion between matrix and porogen, as already verified by SEM images of the cross-sections (Fig. 2), resulting in defects as large as salt particles.

In combination with the increase in elastic modulus, there is a reduction in breaking stress and elongation at break, as a result of the inability of systems to deform (Table 3). This is likely due to the salt particles that can also create weak points or stress concentration zones within the material, increasing the possibility of fractures. The general increase in stiffness and brittleness could cause problems in the MEX 3D printing process; however, the properties are sufficiently compatible with Material Extrusion additive manufacturing process, in fact it was accomplished in all cases, with good quality of printed devices.

After establishing the actual possibility of printing extruded filaments, the first printing tests were carried out. Standard polyamide filaments are notoriously difficult to print for many reasons, such as high printing temperatures and difficult adhesion of the layers [46]. For these reasons, anticipating a further increase in the difficulty of printing PA6/NaCl blends, preliminary printing tests were conducted on extruded PA6 filaments. The printing parameters were established confronting with scientific literature [46–49]. Results are shown in Table 5.

The optimal process parameters that ensured good sample quality are those of Test 4: T nozzle of 250 °C, T plate of 80 °C, extrusion flow rate of 35 mm3/s, printing speed of 10 mm/s; in addition, to promote adhesion between the specimen and the plate, a layer of glue stick was applied to the latter [50, 51]. The same parameters were used for printing the extruded PA6/NaCl mixtures, with slight differences in the extrusion flow rate, adjusted to improve the quality of the devices. In addition, to further optimise adhesion with the plate, a rough plate was used [50]. Process parameters for PA6/NaCl printing are shown in Table 2.

After producing the devices in all blends, they were leached and dried in the way described above. As first inspection, the morphology of the final devices sections and lateral surfaces, and the corresponding pores diameter distributions histograms, are shown in Fig. 5.

In particular, Fig. 6a–c shows cross-sections of the HD_A, HD_B and HD_C leached devices and Fig. 6a'–c' shows the lateral surfaces of the same leached devices. Pores appear well distributed in the sections and the range of pore diameters distribution in histograms remains similar to that prior to printing, for each sample. These results are consistent with the ones obtained for the filaments and demonstrate that the pores have a predictable size in all blends, even after printing. A summary of the pores and porogen statistics based index of the distribution in the systems is reported in Table S1. In lateral surfaces it is evident that the pores have smaller diameters than the sections, as in the case of extrusion, likely due to lateral migration of the particles, which also occurs in the printer nozzle, as already stated in filaments characterization. There is no porogen trace in the images, as expected, so it can be concluded that the leaching of the devices was also substantially complete, in agreement with what observed about the filaments. In order to have further information about pores distribution and architecture in the devices, Mercury Intrusion Porosimetry (MIP) tests were also carried out using Thermo Electron Corporations MIP apparatus and the outcomes are shown in Fig. S2 for leached HD_A. As it can be clearly seen, the test appears to be not adequate and, on the contrary, somehow misleading. This measure, in fact, identify pores with dimension smaller than that previously found by image analysis, i.e., obtained by their direct observation. This condition, apparently strange, has been already observed in our previous work

Table 5 Process parameters identification for PA6 3D Printing

	T nozzle [°C]	T plate [°C]	Flow rate mm3/s	Speed mm/s	Glue	Rough Plate	Result
Test 1	250	80	25	50	-	-	The sample comes off the plate. Poor quality
Test 2	250	80	32.5	16.5	-	-	The sample comes off the plate. Better quality
Test 3	250	80	35	10	-	-	The sample comes off the plate. Good quality
Test 4	250	80	35	10	+	-	The sample does not come off the plate. Good quality

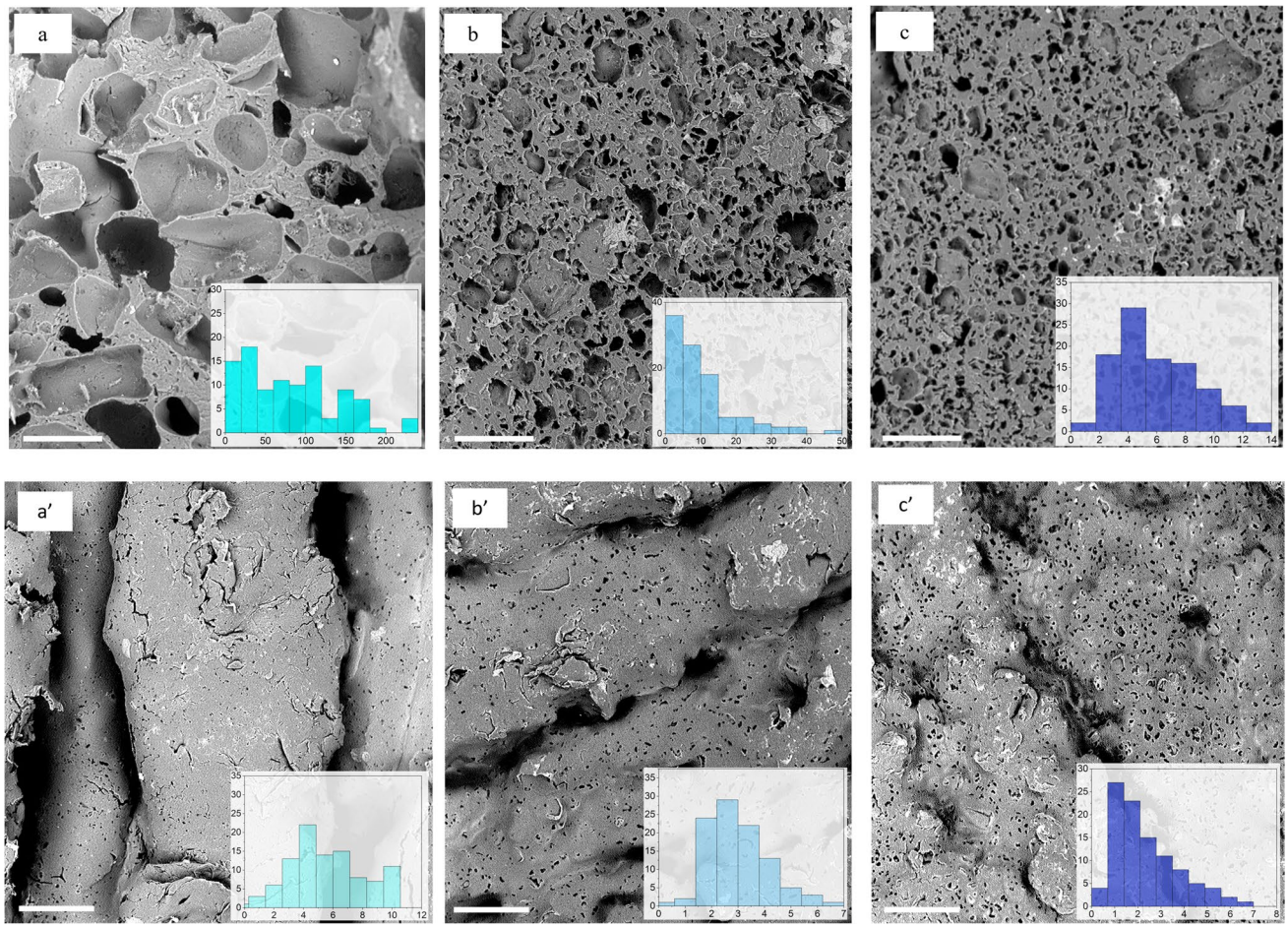

Fig. 5 SEM images of leached printed devices sections (**a**—**c**), lateral surfaces (a' – c') and histograms of pores diameters distribution: HD_A leached (a, a'), HD_B leached (b, b'), HD_C leached (c, c'). Scale bar is 100 µm

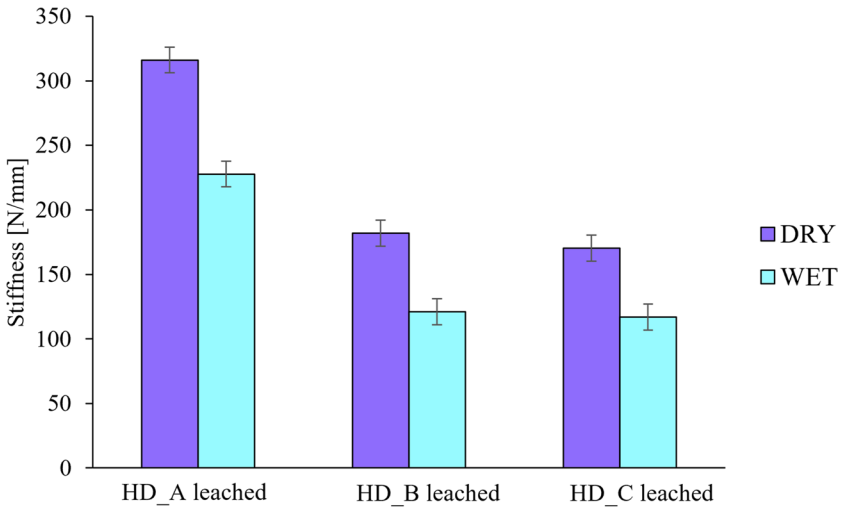

Fig. 6 Stiffness of leached devices HD_A, HD_B and HD_C in dry and in wet conditions

[26], and it has been explained considering that the pores resulting from salt leaching are not perfectly cylindrical, often merged in apparently largest ones and, in addition, arranged so that the smallest pores are on lateral surfaces: this can significantly alter the results and, in particular, it can cause underestimation of pore dimension. So, in this contest, image analysis proves to be the simplest and most appropriate method for analysing pore size distribution.

The porosity of the devices was evaluated as a parameter to quantify successful leaching for all devices and results are reported in Table 6.

P_{Th} was obtained by Eq. 2; it does not take into account the different morphology of the systems, in fact it is identical for all devices and represents the case of complete leaching. The real porosity P_{Grav} was assessed by gravimetric test and by Eq. 3, as a first comparison with P_{Th}. There are specific results for each device and they are all very close to P_{Th} value: it confirms the effectiveness of leaching. Pycnometry was used as further confirmation: again, the real porosity values P_{Pycno} for each device are close to P_{Th} and to P_{Grav}. All this information allows to demonstrate a complete removal of the porogen, as already visually assumed by SEM morphological investigation, hence the effectiveness of the proposed processing in the production of porous systems.

Once the feasibility of producing hollow devices with controlled porosity has been established, their handling is tested, considering the need to mechanically fill, seal and use them as controlled release devices. For this reason, compression tests were performed on leached devices in air (dry) and in distilled water at 37 °C (wet), aiming to simulate the compressive stress conditions to which the samples could be subjected under operational conditions and different humidity and temperature in the environment. It is a well known theory that the presence of pores significantly changes the mechanical properties of materials [52]. So, it is useful to conduct a comparison between the stiffnes of devices in longitudinal direction in dry case and in wet case, assuming that the specimen is subjected to limited stresses during operational conditions in longitudinal direction, which will correspond to the elastic area. Results are shown in Fig. 6.

Mechanical tests showed a strong correlation between pore size and mechanical behavior, as already seen in tensile properties. In this case, the trend of stiffenss is decreasing as the pore size decreases, according to our previous work [16], both in dry and in wet conditions. In detail, the pore size strongly influences the pore density per unit area, but also the wall thickness around the pores. In particular, considering devices with the same porosity, a device with smaller pores (HD_C) has a higher pore density per unit volume and thinner walls when compared to a material with larger pores diameter (HD_A). Consequently, the presence of smaller pores can lead to a greater reduction in the material's ability to resist to compressive loads, reducing its stiffness. It can be seen that HD_B and HD_C exhibit very similar behavior, as expected given their similar morphology. Finally, it is useful to make a comparison of stiffness between the dry and wet cases, in fact stiffness values are always lower in the latter. This is justified by the effect of solution and temperature, that make the material less rigid, causing plasticization of the polymer [16]. Given the two limit conditions, intermediate values are expected for intermediate conditions.

Table 6 Comparison between theoretical porosity (2) and real porosity obtained by gravimetric tests (3) and pycnometry (4)

	P_{Th}	P_{Grav}	P_{Pycno}
HD_A Leached	55.19%	55.01%	55.12%
HD_B Leached	55.19%	55.03%	54.29%
HD_C Leached	55.19%	55.11%	55.19%
Eqs	*2*	*3*	*4*

The devices appear to be suitable for substance loading and sealing, therefore, after being filled with methylene blue (MB) as a model molecule, controlled release kinetics were evaluated to demonstrate that the devices are indeed suitable for releasing substances in a predictable manner. The kinetics of MB release from the devices is shown in Fig. 7.

For all the systems, the release is characterised by three phases: a burst release in the early stages of immersion, a second phase characterized by the progressive depletion of the molecules model in the reservoir, and a final plateau region. In particular, HD_A, HD_B and HD_C show a release of 14%, 7%, and 4%, respectively, after 4 h, followed by a sustained release until the plateau region is reached. The difference in the release kinetics can be attributed to the different pore morphology: HD_A has larger pores than HD_B and HD_C, in fact it releases larger amounts of MB in shorter time. Tests confirm the interconnection of the pores in the device walls, since there is indeed an exchange of matter between inside and outside, for all devices, regardless of the amount of MB released. The different kinetics obtained also confirm the possibility of tailoring the release by varying the morphology of the pores, just by changing the grain size of the porogen.

To evaluate the MB release mechanism, the release data obtained were fitted to zero order, first order, Higuchi and Korsmeyer-Peppas models (Fig. S3). Specifically, the zero-order model represents the case of constant rate and concentration independent release, in the first order model the release rate is proportional to the concentration of the substance in the system, the Higuchi model indicates release controlled by a diffusion process, and finally the Korsmeyer-Peppas model combines various release mechanisms. According to R^2 values, Korsmeyer-Peppas mathematical model better fits the experimental data (Table S2).

In the Korsmeyer-Peppas model is possible to obtain information about the release mechanism, by analysing n value, which is related to the geometry of the device and the release mode. In fact, $0 < n < 0.5$ is representative of systems characterized by diffusive regime with hampered release, $n = 0.5$ is representative of kinetics where Fickian diffusion is the main release mechanism and for this reason the model overlaps with Higuchi's, $0.5 < n < 1$ is the case of anomalous transport, characteristic of those case where in addition to

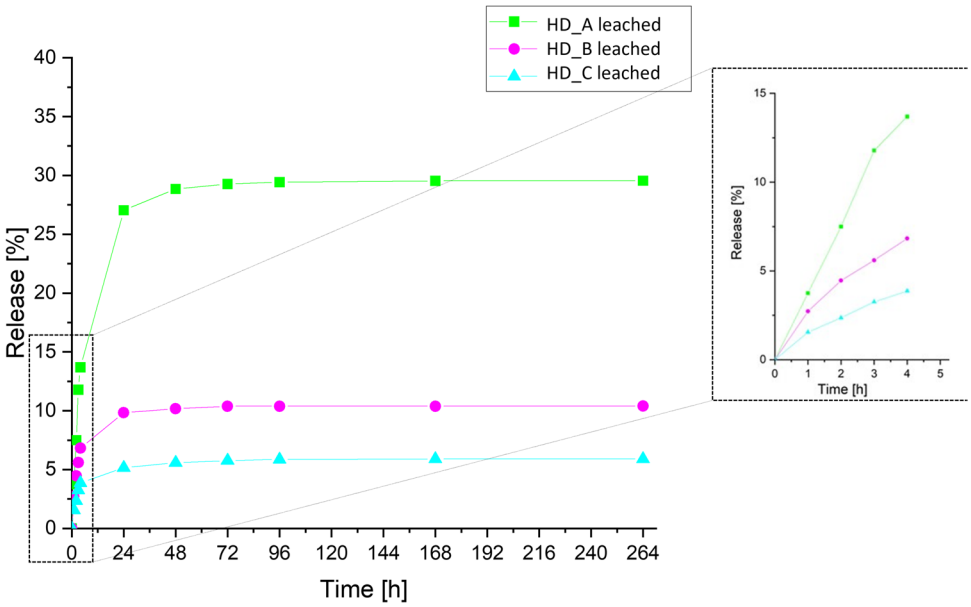

Fig. 7 Release kinetics of MB from HD_A, HD_B and HD_C in distilled water at 25 °C

diffusion other mechanism contribute to release, such as swelling or pores, $n = 1$ indicates a non-Fickian transport and it corresponds to a zero order kinetics and, finally, $n > 1$ is the extreme form of transport representative of severe modifications of matrix [53, 54].

Values of k_P and n of the different systems were then reported in Fig. 8.

The results show that n is between 0.5 and 1 for all devices, so the release mechanism is anomalous and it could be influenced by various factors such as swelling of the hydrophilic polymer and the porosity of the devices. In particular, HD_A is characterized by faster kinetics ($n = 0.96$), attributable to the presence of larger pores and, in fact, HD_B and HD_C show slower kinetics due to smaller pores and kinetics governed more by diffusion [55]. In line with what is expected, in the latter two cases where the release process approaches diffusion (HD_B and HD_C), Higuchi's model also fits the data quite well ($R^2 \approx 0.99$, see Table S1), but Korsmeyer-Peppas model is still better, in fact $n > 0.5$ and other processes are also added to diffusion, as explained above.

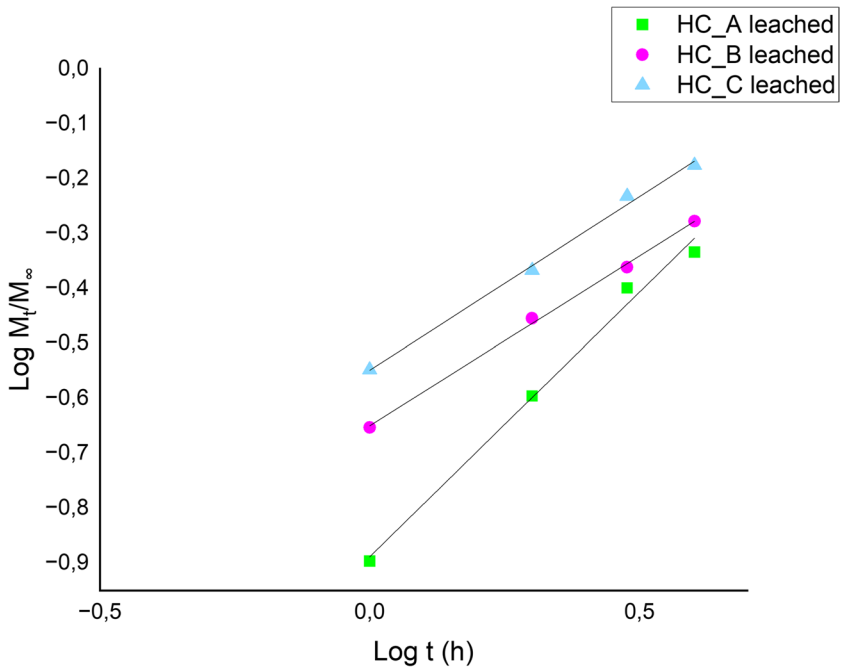

Fig. 8 Logarithmic plot of the release data of MB and values of slopes (n) and intercepts (k) of fitting of Peppas-Korsmeyer model power law applied to the release data collected in the burst region ($M_t/M_\infty < 60\%$)

4 Conclusions

An innovative, cost-effective, and rapid method for producing porous hollow devices has been proposed, by combining melt and wet processing, namely the versatility of Material Extrusion (MEX) additive manufacturing process and the simplicity of salt leaching. Blends with a high porogen content (PA6/NaCl 30/70%wt) and with three different porogen particle sizes were tested in order to assess the possibility of obtaining predictable pore morphologies and high porosity percentages. All blends exhibited rheological and mechanical behavior sufficiently suitable for 3D printing: in fact, the final devices were successfully manufactured, using all prepared formulations. The porogen showed good dispersion in both the filaments and the printed devices, and the pores appeared well distributed in the cross-sections after leaching. Pore distribution range was consistent with the distribution range of the three salt samples, so the morphology of the systems is predictable and adjustable. An interesting decrease in particles and pores size was found in all lateral surfaces, which can be attributed to the fluid dynamics of the porogen inside the extruder and printer nozzle: this is an interesting phenomenon, in fact a porosity gradient could be spontaneously generated along the cross-sections. Printed devices after leaching showed high percentages of real porosity, similar to theoretical porosity, a quantitative symptom of total leaching. Despite the high degree of voids, they have maintained sufficient compressive mechanical properties, even in wet conditions, so the devices were confirmed as possible to handle and suitable for the application. Hollow devices were filled with methylene blue (MB) as model molecule, to test the functionality of the devices in releasing in a controlled manner. MB's release tests demonstrated the interconnection of the pores in the wall of the devices and the different kinetics confirm the possibility of tailoring the release through the morphology of the device pores, i.e., through the granulometry of the porogen. The Peppas-Korsmeyer model showed that the release mechanism for all devices is anomalous, thus influenced by swelling and porosity, and confirmed faster kinetics for the devices with the largest pores. These properties would allow the controlled release of other molecules, such as drugs, fertilizers, and pesticides, confirming the versatility of the process. Finally, the use of MEX would also allow to modified the shape of the devices for other applications, where porosity control is crucial, even creating extremely elaborate geometries with large surface area, while considering the technological limitations of the printer.

Supplementary Information The online version contains supplementary material available at https://doi.org/10.1007/s42114-025-01255-8.

Acknowledgements This research was funded by SiciliAn MicronanOTecH Research Additionally, Innovation Center —SAMOTHRACE, European Commission ECS00000022, CUP: B73C22000810001. Authors gratefully acknowledge the financial support provided by the Italian Ministry of Education, University and Research (MIUR) under the PRIN2022—P20228WNZ2Z. This study was carried out within the MICS (Made in Italy – Circular and Sustainable) Extended Partnership and received funding from the European Union Next-GenerationEU (PIANO NAZIONALE DI RIPRESA E RESILIENZA (PNRR) – MISSIONE 4 COMPONENTE 2, INVESTIMENTO 1.3 – D.D. 1551.11-10-2022, PE00000004). This manuscript reflects only the authors' views and opinions, neither the European Union nor the European Commission can be considered responsible for them.

Author contribution M.B.: Data curation; Investigation; Methodology; Visualization; Roles/Writing—original draft; and Writing—review & editing. M.C.M.: Conceptualization; Data curation; Formal analysis; Investigation; Methodology; Supervision; Visualization; Roles/Writing—original draft; and Writing—review & editing. R.S.: Conceptualization; Data curation; Formal analysis; Funding acquisition; Investigation; Methodology; Resources; Supervision; Validation; Visualization; Roles/Writing—original draft; and Writing—review & editing.

Funding Open access funding provided by Università degli Studi di Palermo within the CRUI-CARE Agreement. This research was funded by SiciliAn MicronanOTecH Research Additionally, Innovation Center —SAMOTHRACE, European Commission ECS00000022, CUP: B73C22000810001. Authors gratefully acknowledge the financial support provided by the Italian Ministry of Education, University and Research (MIUR) under the PRIN2022—P20228WNZ2Z. This study was carried out within the MICS (Made in Italy – Circular and Sustainable) Extended Partnership and received funding from the European Union Next-GenerationEU (PIANO NAZIONALE DI RIPRESA E RESILIENZA (PNRR) – MISSIONE 4 COMPONENTE 2, INVESTIMENTO 1.3 – D.D. 1551.11–10-2022, PE00000004). This manuscript reflects only the authors' views and opinions, neither the European Union nor the European Commission can be considered responsible for them.

Data availability Data sets generated during the current study are available from the corresponding author on reasonable request.

Declarations

Conflict of interest The authors declare no competing interests.

References

1. Wang A, Ma Y, Zhao D (2024) Pore engineering of porous materials: effects and applications. ACS Nano 18:22829–22854

2. Sivasankarapillai VS, Sundararajan A, Eswaran M, Dhanusuraman R (2024) Hierarchical porous activated carbon derived from callistemon viminalis leaf biochar for supercapacitor and methylene blue removal applications. ES Energy and Environment 24. https://doi.org/10.30919/esee1124
3. Liu T, Wang Y, Kuang T (2024) Oriented porous polymer scaffolds in tissue engineering: a comprehensive review of preparation strategies and applications. Macromol Mater Eng 309(1):2300246. https://doi.org/10.1002/mame.202300246
4. Scaffaro R, Mistretta MC, Balsamo M (2024) Innovative 3D-printed devices for water pollutant removal: Comprehensive review on printing parameters, composition, properties and performances of the latest 3D-systems. Polym Test 140:108627. https://doi.org/10.1016/j.polymertesting.2024.108627
5. Adepu S, Ramakrishna S (2021) Controlled drug delivery systems: Current status and future directions. Molecules 26(19):5905
6. Berney T, Wassmer CH, Lebreton F, Bellofatto K, Fonseca LM, Bignard J, Hanna R, Peloso A, Berishvili E (2022) From islet of Langerhans transplantation to the bioartificial pancreas. Presse Med 51:104139. https://doi.org/10.1016/j.lpm.2022.104139
7. Duan Q, Jiang S, Chen F, Li Z, Ma L, Song Y, Yu X, Chen Y, Liu H, Yu L (2023) Fabrication, evaluation methodologies and models of slow-release fertilizers: A review. Ind Crops Prod 192:116075
8. Singh G, Ramadass K, Sooriyakumar P, Hettithanthri O, Vithange M, Bolan N, Tavakkoli E, Van Zwieten L, Vinu A (2022) Nanoporous materials for pesticide formulation and delivery in the agricultural sector. J Control Release 343:187–206
9. Pavithran RK, Reddy SG, Siva Kumar B, Kugabalasooriar S (2024) Enhancing sustainability in agriculture: natural polymer-based controlled release systems for effective pest management and environmental protection. ES Food and Agroforestry 18. https://doi.org/10.30919/esfaf1276
10. Borandeh S, van Bochove B, Teotia A, Seppälä J (2021) Polymeric drug delivery systems by additive manufacturing. Adv Drug Deliv Rev 173:349–373. https://doi.org/10.1016/j.addr.2021.03.022
11. Korelidou A, Domínguez-Robles J, Magill ER, Eleftheriadou M, Cornelius VA, Donnelly RF, Margariti A, Larrañeta E (2022) 3D-printed reservoir-type implants containing poly(lactic acid)/poly(caprolactone) porous membranes for sustained drug delivery. Biomaterials Advances 139. https://doi.org/10.1016/j.bioadv.2022.213024
12. Farina M, Chua CYX, Ballerini A, Thekkedath U, Alexander JF, Rhudy JR, Torchio G, Fraga D, Pathak RR, Villanueva M, Shin CS, Niles JA, Sesana R, Demarchi D, Sikora AG, Acharya GS, Gaber AO, Nichols JE, Grattoni A (2018) Transcutaneously refillable, 3D-printed biopolymeric encapsulation system for the transplantation of endocrine cells. Biomaterials 177:125–138. https://doi.org/10.1016/j.biomaterials.2018.05.047
13. Cano-Vicent A, Tambuwala MM, SkS H, Barh D, Aljabali AAA, Birkett M, Arjunan A, Serrano-Aroca Á (2021) Fused deposition modelling: Current status, methodology, applications and future prospects. Addit Manuf 47:102378. https://doi.org/10.1016/j.addma.2021.102378
14. Manjunath KS, Sridhar K, Gopinath V, Sankar K, Sundaram A, Gupta N, Shiek ASSJ, Shantanu PS (2021) Facile manufacturing of fused-deposition modeled composite scaffolds for tissue engineering—an embedding model with plasticity for incorporation of additives. Biomed Mater 16:015028. https://doi.org/10.1088/1748-605X/abc1b0
15. Buj-Corral I, Bagheri A, Petit-Rojo O (2018) 3D printing of porous scaffolds with controlled porosity and pore size values. Materials 11. https://doi.org/10.3390/ma11091532
16. Scaffaro R, Lopresti F, Botta L, Rigogliuso S, Ghersi G (2016) Preparation of three-layered porous PLA/PEG scaffold: relationship between morphology, mechanical behavior and cell permeability. J Mech Behav Biomed Mater 54:8–20. https://doi.org/10.1016/j.jmbbm.2015.08.033
17. Prasad A, Sankar MR, Katiyar V (2017) State of Art on Solvent Casting Particulate Leaching Method for Orthopedic Scaffolds-Fabrication. Mater Today Proc 4:898–907. https://doi.org/10.1016/j.matpr.2017.01.101
18. Wu J, Hong Y (2016) Enhancing cell infiltration of electrospun fibrous scaffolds in tissue regeneration. Bioact Mater 1:56–64
19. Yahay Z, Tolabi H, Delavar F, Poursamar SA, Mirhadi SM, Tavangarian F (2023) Fabrication of meso/macroporous TiO2/PCL composite scaffolds by direct ink writing: The effects of porogen content on the compressive modulus and in vitro behavior. Mater Today Commun 35. https://doi.org/10.1016/j.mtcomm.2023.105769
20. Kashyap D, Kishore Kumar P, Kanagaraj S (2018) 4D printed porous radiopaque shape memory polyurethane for endovascular embolization. Addit Manuf 24:687–695. https://doi.org/10.1016/j.addma.2018.04.009
21. González-Henríquez CM, Rodríguez-Umanzor FE, Acuña-Ruiz NF, Vera-Rojas GE, Terraza-Inostroza C, Cohn-Inostroza NA, Utrera A, Sarabia-Vallejos MA, Rodríguez-Hernández J (2022) Fabrication and Testing of Multi-Hierarchical Porous Scaffolds Designed for Bone Regeneration via Additive Manufacturing Processes. Polymers (Basel) 14:4041. https://doi.org/10.3390/polym14194041
22. Teerasuchai K, Ksapabutr B, Panapoy M, Chaiyut N (2023) Preparation and properties of poly(butylene succinate) porous scaffold by fused deposition modeling and salt leaching techniques. J Curr Sci Technol 11:334–341
23. Kosorn W, Wutticharoenmongkol P (2021) Poly(ε-caprolactone)/Poly(3-hydroxybutyrate-co-3-hydroxyvalerate) blend from fused deposition modeling as potential cartilage scaffolds. Int J Polym Sci 2021:1–18. https://doi.org/10.1155/2021/6689789
24. Aydin MS, Marek N, Luciani T, Mohamed-Ahmed S, Lund B, Gjerde C, Mustafa K, Suliman S, Rashad A (2024) Impact of porosity and stiffness of 3d printed polycaprolactone scaffolds on osteogenic differentiation of human mesenchymal stromal cells and activation of dendritic cells. ACS Biomater Sci Eng. https://doi.org/10.1021/acsbiomaterials.4c01108
25. Wang SJ, Deng RH, Song CH, Yuan FZ, Li PQ, Cao XY, Wang X, Lin L, Zhang JY, Zhu YF, Yu JK (2024) Biomechanically matched and multistage hybrid porous scaffolds for stem cell-based osteochondral regeneration. Nano Today 59. https://doi.org/10.1016/j.nantod.2024.102539
26. Scaffaro R, Re G Lo, Rigogliuso S, Ghersi G (2012) 3D polylactide-based scaffolds for studying human hepatocarcinoma processes in vitro. Sci Technol Adv Mater 13. https://doi.org/10.1088/1468-6996/13/4/045003
27. Felder S, Vu NA, Reese S, Simon JW (2020) Modeling the effect of temperature and degree of crystallinity on the mechanical response of Polyamide 6. Mechanics of Materials 148. https://doi.org/10.1016/j.mechmat.2020.103476
28. Millot C, Fillot LA, Lame O, Sotta P, Seguela R (2015) Assessment of polyamide-6 crystallinity by DSC: Temperature dependence of the melting enthalpy. J Therm Anal Calorim 122:307–314. https://doi.org/10.1007/s10973-015-4670-5
29. Scaffaro R, Lopresti F, Botta L, Maio A, Sutera F, Mistretta MC, La Mantia FP (2016) A facile and eco-friendly route to fabricate poly(lactic acid) scaffolds with graded pore size. J Vis Exp. https://doi.org/10.3791/54595
30. Bueno-López C, Tamarit-Martínez C, Alambiaga-Caravaca AM, Balaguer-Fernández C, Merino V, López-Castellano A, Rodilla V (2021) 3d printing of temporary prostheses for controlled-release of drugs: Design, physical characterization

and preliminary studies. Pharmaceuticals 14. https://doi.org/10.3390/ph14121240
31. Scaffaro R, Settanni L, Gulino EF (2023) Release profiles of carvacrol or chlorhexidine of pla/graphene nanoplatelets membranes prepared using electrospinning and solution blow spinning: a comparative study. Molecules 28. https://doi.org/10.3390/molecules28041967
32. Unagolla JM, Jayasuriya AC (2018) Drug transport mechanisms and in vitro release kinetics of vancomycin encapsulated chitosan-alginate polyelectrolyte microparticles as a controlled drug delivery system. Eur J Pharm Sci 114:199–209. https://doi.org/10.1016/j.ejps.2017.12.012
33. Kanehl P, Stark H (2015) Hydrodynamic segregation in a bidisperse colloidal suspension in microchannel flow: A theoretical study. J Chem Phys 142. https://doi.org/10.1063/1.4921800
34. Acierno D, Patti A (2023) Fused Deposition Modelling (FDM) of Thermoplastic-based filaments: process and rheological properties—an overview. Materials 16(24):7664. https://doi.org/10.3390/ma16247664
35. Ceraulo M, Botta L, Scaffaro R, Mistretta MC, La Mantia FP (2014) Prediction of the flow curves of thermoplastic polymer/clay systems from torque data. Polym Test 37:12–18. https://doi.org/10.1016/j.polymertesting.2014.04.003
36. Puch F, Hopmann C (2014) Nylon 6/multiwalled carbon nanotube composites: effect of the melt-compounding conditions and nanotube content on the morphology, mechanical properties, and rheology. J Appl Polym Sci 131. https://doi.org/10.1002/app.40893
37. Scaffaro R, Citarrella MC, Gulino EF, Morreale M (2022) Hedysarum coronarium-based green composites prepared by compression molding and fused deposition modeling. Materials 15. https://doi.org/10.3390/ma15020465
38. Scaffaro R, Botta L, Maio A, Mistretta MC, La Mantia FP (2016) Effect of graphene nanoplatelets on the physical and antimicrobial properties of biopolymer-based nanocomposites. Materials 9. https://doi.org/10.3390/ma9050351
39. Botta L, Scaffaro R, Mantia FPLA, Dintcheva NT (2010) Effect of different matrices and nanofillers on the rheological behavior of polymer-clay nanocomposites. J Polym Sci B Polym Phys 48:344–355. https://doi.org/10.1002/polb.21896
40. Scaffaro R, Maio A, Botta L, Gulino EF, Gulli D (2019) Tunable release of Chlorhexidine from Polycaprolactone-based filaments containing graphene nanoplatelets. Eur Polym J 110:221–232. https://doi.org/10.1016/j.eurpolymj.2018.11.031
41. Scaffaro R, La Mantia FP, Botta L, Morreale M, Dintcheva NT, Mariani P (2009) Competition between chain scission and branching formation in the processing of high-density polyethylene: Effect of processing parameters and of stabilizers. Polym Eng Sci 49:1316–1325. https://doi.org/10.1002/pen.21317
42. Maio A, Gammino M, Gulino EF, Megna B, Fara P, Scaffaro R (2020) Rapid One-Step Fabrication of Graphene Oxide-Decorated Polycaprolactone Three-Dimensional Templates for Water Treatment. ACS Appl Polym Mater 2:4993–5005. https://doi.org/10.1021/acsapm.0c00852
43. Li J, Leng J, Jiang Y, Zhang J (2021) Experimental characterization of 3D printed PP/h-BN thermally conductive composites with highly oriented h-BN and the effects of filler size. Compos Part A Appl Sci Manuf 150. https://doi.org/10.1016/j.compositesa.2021.106586
44. Arrigo R, Frache A (2022) FDM Printability of PLA Based-Materials: The Key Role of the Rheological Behavior. Polymers (Basel) 14. https://doi.org/10.3390/polym14091754
45. Liu Z, Qiu J, Shi Z, Zhang S, Xing H, Li M, Shi Y, Tang T (2020) Adjusting cell structure of polypropylene composite foams by controlling the size and dispersed state of NaCl particles during CO2 batch foaming process. Polymer (Guildf) 194. https://doi.org/10.1016/j.polymer.2020.122406
46. Squires AD, Lewis RA (2018) Feasibility and Characterization of Common and Exotic Filaments for Use in 3D Printed Terahertz Devices. J Infrared Millim Terahertz Waves 39:614–635. https://doi.org/10.1007/s10762-018-0498-y
47. Buj-Corral I, Zayas-Figueras EE (2023) Comparative study about dimensional accuracy and form errors of FFF printed spur gears using PLA and Nylon. Polym Test 117:107862. https://doi.org/10.1016/j.polymertesting.2022.107862
48. Lay M, Thajudin NLN, Hamid ZAA, Rusli A, Abdullah MK, Shuib RK (2019) Comparison of physical and mechanical properties of PLA, ABS and nylon 6 fabricated using fused deposition modeling and injection molding. Compos B Eng 176:107341. https://doi.org/10.1016/j.compositesb.2019.107341
49. Luo M, Huang S, Man Z, Cairney JM, Chang L (2022) Tribological behaviour of fused deposition modelling printed short carbon fibre reinforced nylon composites with surface textures under dry and water lubricated conditions. Friction 10:2045–2058. https://doi.org/10.1007/s40544-021-0574-5
50. Chapman G, Pal AK, Misra M, Mohanty AK (2021) Studies on 3D printability of novel impact modified nylon 6: experimental investigations and performance evaluation. Macromol Mater Eng 306. https://doi.org/10.1002/mame.202000548
51. Al Mortadi NA, Al Husein BA, Alzoubi KH, Khabour OF, Eggbeer D (2022) Cytotoxicity of 3D printed materials for potential dental applications: an in vitro study. Open Dent J 16. https://doi.org/10.2174/18742106-v16-e2112230
52 Al-Maharma AY, Patil SP, Markert B (2020) Effects of porosity on the mechanical properties of additively manufactured components: a critical review. Mater Res Express 7(12):122001
53. Scaffaro R, Maio A, Gulino EF, Micale GDM (2020) PLA-based functionally graded laminates for tunable controlled release of carvacrol obtained by combining electrospinning with solvent casting. React Funct Polym 148. https://doi.org/10.1016/j.reactfunctpolym.2020.104490
54. Scaffaro R, Citarrella MC, Gulino EF (2022) Opuntia Ficus Indica based green composites for NPK fertilizer controlled release produced by compression molding and fused deposition modeling. Compos Part A Appl Sci Manuf 159. https://doi.org/10.1016/j.compositesa.2022.107030
55. Ju T, Gaisford S, Williams GR (2024) Ciprofloxacin-loaded electrospun nanofibres for antibacterial wound dressings. J Drug Deliv Sci Technol 91. https://doi.org/10.1016/j.jddst.2023.105264